Available online at www.sciencedirect.com
SCIENCE DIRECT
Diamond & Related Materials 14 (2005) 913–920
DIAMOND AND RELATED MATERIALS
www.elsevier.com/locate/diamond

The smoothness of tetrahedral amorphous carbon

C. Casiraghi*, A.C. Ferrari, J. Robertson

Department of Engineering, University of Cambridge, Trumpington Street, Cambridge CB2 1PZ, UK

Available online 11 March 2005

Abstract

Diamond-like Carbon (DLC) is the preferred coating material for magnetic storage disks and future optical storage devices. Tetrahedral amorphous carbon (ta-C) films are used to coat the read heads. Films with a thickness below 2 nm and roughness well below 1 nm are needed to achieve the desired storage densities. To reach these values, we must determine the minimum thickness for continuous and pin-hole free films. Here, we review the studies on the smoothness and the growth mechanism of ta-C. The film roughness R of every growing surface generally increases with the thickness z as $R\sim z^{\beta}$ until saturation. For a fixed thickness, R increases with the lateral scale length L as $R\sim L^{\alpha}$. The exponents α and β are called roughness and growth exponents, respectively, and they are uniquely defined by the growth process. The roughness evolution of ta-C films grown at room temperature was measured by atomic force microscopy. The roughness is very low (~0.12 nm) and the growth exponents are $\alpha\sim0.39$ and $\beta\sim0$–0.1. These require the presence of surface diffusion and relaxation. We propose that the diffusion is local and it occurs during the thermal spike, which accompanies ion dominated depositions. Monte Carlo simulations confirm this and show low exponents consistent with experiments. Thus, the scaling analysis shows that the surface properties, for a fixed temperature and ion energy, are a separate process to subplantation, which determines the sp^3 bonding of the bulk film.
© 2005 Elsevier B.V. All rights reserved.

Keywords: Tetrahedral amorphous carbon; Surface properties; Nucleation

1. Introduction

Diamond-like Carbon (DLC) is the name attributed to a variety of amorphous carbon materials containing a large fraction of sp^3 bonds [1]. The sp^3 fraction can vary from 0 to 90%, depending on the deposition method [1] and it determines the density and the mechanical properties [2]. The term tetrahedral amorphous carbon (ta-C) designates a non-hydrogenated carbon containing a high fraction of sp^3 bonded carbon. Thus, ta-C is the DLC with the best mechanical properties [1,2].

In recent years, there have been important advances in the science of carbon such as the development of the chemical vapour deposition of diamond [3] and the discovery of C_{60} [4] and carbon nanotubes [5]. Similarly, DLC has become increasingly important from a technological point of view. For example, DLC is a key component of the data storage industry, both magnetic and optical, where developments of the DLC protective layer could allow increases of the data storage density to ~1 Tbit/in^2 and ~100 Gbit/in^2, respectively [6–11].

Magnetic storage technology has used DLC coatings for 20 years to protect the head and disk from wear and corrosion. The coatings presently used are sputtered amorphous carbon films, typically containing a significant fraction of nitrogen (a-C:N) or hydrogen (a-C:H) and thickness of 3–5 nm [12–14]. A key aspect of magnetic storage technology is that data storage density is presently doubling every year [6,7]. The ultimate barrier to storage density is the super-paramagnetic limit, where the thermal energy is able to overcome the coercive energy of the magnetic bit. For longitudinal recording this limit is ~100 Gbit/in^2 [6,7] while vertical recording may allow storage densities up to ~1 Tbit/in^2 [7,8]. Both cases require the read head to approach close to the magnetic layer and the use of ever-thinner layers of DLC 1–2 nm thick [6–10] (Fig. 1). The main role of the DLC coating is to provide a corrosion barrier to the recording medium, so they must be atomically smooth, dense, continuous and pin-hole free.

* Corresponding author. Tel.: +44 1223 765242; fax: +44 1223 332662.
E-mail address: cc324@eng.cam.ac.uk (C. Casiraghi).

0925-9635/$ - see front matter © 2005 Elsevier B.V. All rights reserved.
doi:10.1016/j.diamond.2005.01.023

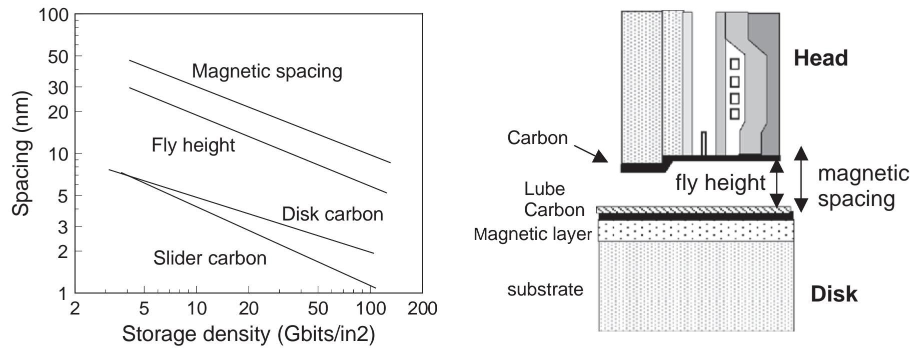

Fig. 1. Variation of carbon thickness on disk and sliders, magnetic spacing and fly height with storage density according to the roadmap for magnetic storage technology. Films with thickness of 1–2 nm are needed in order to reach storage density over 100 Gbit/in^2.

However, both a-C:N and a-C:H cease to provide protection against corrosion and wear below about 3 nm because they are not continuous [8,15]. Actually, the low ion energy (~5 eV) involved in the magnetron sputtering [15] cannot overcome any nucleation barriers. Thus, an improved coating for future hard disks is needed. The coating must be continuous and very smooth, even at ultra-low thickness. A good candidate is ta-C, because of its unique combination of desirable properties, such as atomic smoothness, wear resistance, and compatibility to the lubricant [1,10,16,17].

We have noted that the coverage is the most important requirement for storage disks. However, the surface properties of ta-C are not well known. The roughness of ta-C has been studied experimentally as a function of substrate temperature [18] and ion energy [18,19], but in the case of ultra-thin films for hard disk coating, both temperature and ion energy are fixed and only the thickness, i.e. the deposition time, is changed. There are also some molecular simulations on the first stages of ta-C growth [20–22], but they focus only on the sp^3 evolution. Only few calculations focus on the surface [23–25], but the roughness evolution was not studied.

In this paper we review the studies on the roughness kinetics of ta-C, grown at room temperature and fixed ion energy. This allows us to study the film coverage and also to quantify the nucleation and the first stages of growth of ta-C films. A few previous works assessed this problem in other types of carbon films, such as nanostructured carbons [26], some carbon nitrides [27] or hydrogenated amorphous carbons [9].

2. Experimental

Two sets of ta-C films of increasing thickness are investigated: i) ta-C films deposited by a lab scale Filtered Cathodic Vacuum Arc (FCVA) with an integrated off-plane double bend (S-bend) [28]. The deposition rate is ~0.8 nm/s and the film thickness is between 4 and 70 nm as derived by a combination of ellipsometry and X-ray Reflectivity (XRR). The thickness determination by XRR is precise to 0.1 nm [2]. The deposition chamber was evacuated to 10^{-4} Pa using a turbo-molecular pump. No substrate bias was used. The self-bias results in an ion energy of about 20–40 eV. Ta-C films are deposited on silicon (100) substrates previously cleaned with acetone in an ultrasonic bath. This ensures a substrate roughness of ~0.2 nm. Thick samples deposited in these conditions have ~88% sp^3, a density of 3.3 g cm^{-3} and a Young's modulus of ~750 GPa [2,29]. Ultra-thin samples, i.e. with thickness below 10 nm, deposited in these conditions have 50% sp^3, a density of 2.6 g cm^{-3} and a Young's Modulus of 100 GPa [30]. ii) ta-C films deposited by a near-production process filtered high current pulsed arc (HCA) [31]. The deposition rate is 8–10 nm/s and the film thickness is between 1.6 nm and 20 nm as determined by XRR and ellipsometry. The base pressure is ~10^{-4} Pa. The films were deposited at room temperature on ultra-smooth silicon with a roughness of 0.1 nm. Samples deposited in these conditions have a density of ~2.9 g cm^{-3} and a modulus of ~500 GPa [32]. However, ultra-thin samples deposited in these conditions still exhibit ~2.6 g cm^{-3} density and a Young's Modulus of ~100 GPa [32].

Note that in magnetic head coating, the head is pre-coated with a very thin silicon layer. Thus, studying the growth on Si substrates can be compared to real industrial process conditions.

The surface morphology evolution was investigated by Atomic Force Microscopy (AFM). We used a Nanoscope III Digital Instrument AFM operating in tapping mode. We used tips made from etched silicon. The resonant frequency and the length of the cantilever are 254–389 kHz and 160 μm, respectively. A surface scan size of 1 μm×1 μm was used. The root mean square roughness is defined as:

$$R = \left(\sum \frac{(h_i - h_{av})^2}{N} \right)^{1/2} \tag{1}$$

where h_i is the film height, h_{av} is the average of the height values in a given area and N is the number of measurements. R was calculated on a 0.5 μm×0.5 μm area in order to avoid any macro-particles [28]. A total of 254 line scans are taken for each image.

3. Surface properties

The film coverage can be related with different effects: i) extrinsic factors such as substrate cleanliness and filtering of particulates from the film flux; ii) intrinsic factors such as the surface mobility or nucleation barriers. If there is a nucleation barrier, then the film will not nucleate everywhere on the surface. The surface mobility can help the formation of islands since atoms can be free to move across the surface to form islands in order to reduce the surface energy, but leaving some parts of the surface uncovered. On the other hand, diffusion and relaxation phenomena can help surface smoothing. The effect of the diffusion depends on the diffusion length, which in turn depends on the experimental conditions, such as substrate temperature or ion energy [33–35]. Thus, the study of the surface properties achieves the understanding of the basic mechanism leading the roughness, i.e. the growth process.

Fig. 2 shows the schematic variation of roughness with film thickness for a general case. At first, the films consist of a series of islands where the new phase has nucleated, and the roughness increases quickly. Then the roughness peaks and decreases as the islands coalesce to form a closed, continuous film. The third stage consists of a constant roughness for epitaxial films. Finally, the roughness increases gradually above a 'roughening transition'. The third stage is absent in the case of an amorphous film, as here. We shall see that the first two stages are also largely absent for ta-C, because of the lack of nucleation barriers.

It is possible to analyse the increase in roughness in the fourth stage for amorphous or small-grained films, by using fractal models and the scaling theory [36–38]. This considers the importance of the scale of the measurements with regard to the structural characteristics. It assumes that every growing surface is self-affine, so that the surface is

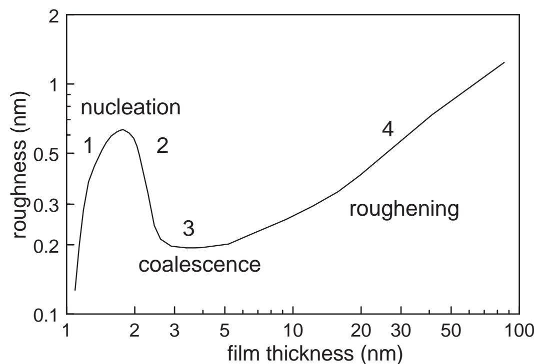

Fig. 2. Schematic of roughness variation with film thickness in a general case. At first, the films consist of a series of islands where the new phase has nucleated, and the roughness increases quickly. Then the roughness peaks and decreases as the islands coalesce to form a closed, continuous film. The third stage consists of a constant roughness for epitaxial films. Finally, the roughness increases gradually above a 'roughening transition'.

invariant under anisotropic transformations [36,37]. This is due to the fact that the surface properties of films deposited under non-equilibrium conditions are determined by the competition between fluctuations and smoothening processes (excluding chemical reactions). In film deposition, the fluctuations derive from the non-uniform nature of the incoming flux: the atoms reach the surface at random positions, with random time interval between them. Random fluctuations take place on both long and short-range scales. On the other hand, smoothing effects, such as thermal diffusion, tend to eliminate the height fluctuations. They occur on a length scale of the atomic diffusion length. Hence, these two processes can only lead to a balancing effect on a relatively short-range scale and a kinetic roughening of the film will occur. Thus, R scales as [36–38]

$$R \sim L^{\alpha} \cdot f\left(t/L^{\alpha/\beta}\right) \tag{2}$$

where t is the deposition time, L is the length scale i.e. $L \times L$ is the window size where R is measured. $f(u)$ is the scaling function of the argument $u = t/L^{\alpha/\beta}$. For small times, that is $u \ll 1$ [35–38]:

$$R \sim t^{\beta} \tag{3}$$

This is the "scaling law" for ultra-thin films, assuming that the deposition rate is constant. Thus, as deposition occurs, the growing surface gradually roughens. Over a certain time, the roughness reaches saturation. For a fixed time [37]:

$$R \sim L^{\alpha} \tag{4}$$

The roughness depends on the length scale accessible to the method probing the surface. Only over a certain length scale, R is constant. The roughness exponent α ($0 \le \alpha \le 1$) is a static exponent since it describes how the sites on the surface are correlated at a certain time. In contrast, the growth exponent β is a dynamic exponent since it determines the first stage of growth (Eq. (3)).

The maximum peak to valley difference, R_a, is generally 5–6 times R. Thus, if z is the ta-C thickness, the film is continuous if the difference "$z-R_a$" remains sizeable as z decreases. However, the scaling analysis contains more information than only the coverage. The exponents α and β are uniquely defined by the growth process. The exponents of some simple discrete models have been calculated [36–38]. In these models the morphology depends on how and where the particle is allowed to come to rest and stick to the existing surface (Fig. 3). For example, in the random deposition the particles stick at the surface and β is 0.5, while α is not defined. In the random deposition with surface diffusion the particles do not stick irreversibly, but can relax to a nearby site with a lower height. This model gives $\beta=1/4$ and $\alpha=1/2$. In the case of ballistic deposition the lateral sticking is allowed, in contrast to the random deposition model. Here the particle sticks to the first site along its

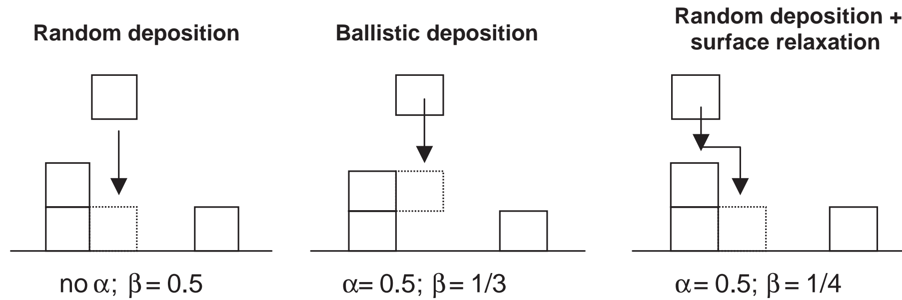

Fig. 3. Example of discrete growth models and their scaling exponents α and β. Their values define the growth mechanism. For random deposition the particles stick at the surface; for random deposition with surface diffusion, the particles do not stick irreversibly, but can relax to a nearby site of lower height. The ballistic deposition is different from the random deposition because the lateral sticking is allowed.

trajectory that has an occupied nearest neighbor. In this case the fractal exponents are β=1/3 and α=1/2. However, the real experiment is much richer in mechanisms leading to roughening. Thus, continuum equations have been proposed [37,39–41]. Table 1 shows the fractal exponents derived from these equations.

Eq. (3) allows us to derive β by plotting ln(R) as a function of ln(z). In order to find α, we must use spatial surface descriptors, since the roughness exponent describes how the sites are correlated as a function of the distance between them, at a certain time. For example the height–height correlation function can be used [36]:

$$H(r,t) = <[h(r,t) - h(0,t)]^2> \quad (5)$$

where r is the radial distance between two sites and $h(r,t)$ is the height of the site at position r and time t. The bracket denotes the spatial average. Below a certain distance, called correlation length (ξ) [36]:

$$H(r,t) \sim r^{2\alpha} \qquad \text{for } r<\xi \quad (6)$$

Thus the roughness exponent can be derived from the initial slope of $H(r,t)$. Furthermore, the growth exponent can be derived from the kinetic evolution of ξ [36,37]. Above ξ, H becomes a constant. As

$$\xi \sim t^{\beta/\alpha} \quad (7)$$

this allows us to calculate the ratio β/α, and from Eq. (6) we find β.

Fig. 4 shows the AFM pictures of ta-C films with thickness a) 1.6 nm deposited by HCA; b) 3 nm by HCA; (c) 15 nm and (d) 60 nm by FCVA. We note that the surface is continuous and characterised by uniformly distributed features. No particular differences in the morphology are visible.

Fig. 5 is a logarithmic plot of the roughness evolution as a function of film thickness. The roughness is approximately constant (R~0.12 nm) for every sample and it is in agreement with previous data on thicker films [19]. In the case of lab scale FCVA films, the roughness shows an apparent increase from 0.12 to 0.17 nm when the film thickness decreases from 8 to 4 nm. This increase could be due to nucleation barriers. In fact, this is due to the initial roughness of the silicon substrate (~0.2 nm), which is smoothed exponentially [42] by the covering ta-C film. The extrinsic origin of this initial roughness is demonstrated by the data from HCA films where no increase is visible due to the much smoother Si substrate (R~0.1 nm).

Fig. 5 shows that R_a is always lower than the film thickness, thus ultra-thin ta-C films are continuous and pin-hole free. This has also been confirmed on large areas by X-ray Photoelectron Spectroscopy measurements. In this case the core levels of the substrate are not seen through the overcoat [43,44]. Fig. 5 also shows that the roughness is independent of thickness, so the growth exponent β is zero.

Fig. 6 shows the height–height correlation function. We derived a roughness exponent α ~0.39 [45]. Eq. (7) gives β/α ~0.24, and so β~0.09 [45], in agreement with Fig. 5.

Table 1
Scaling exponents predicted by the most used continuum growth equations, such as Edwards-Wilkinson (EW) [40], Kardar-Parisi-Zhang (KPZ) [39] and Molecular Beam Epitaxy (MBE) [37]

Model	α	β
EW	0	0
KPZ	~0.38	~0.24
MBE	1	1/4
Non-linear MBE	2/3	1/5

4. Discussion

We found that the scaling exponents for ta-C are: α~0.39 and β~0–0.1. These exponents do not match any of the standard growth mechanisms [37–41]. However, a growth exponent of β~0 generally arises from surface diffusion plus relaxation, as noted by Tamborenea and Das Sarma [46]. These are thermally activated process. Thus, we would expect the low roughness of ta-C to be related with a high temperature.

Ta-C is characterised by a high fraction of sp^3 bonding. The most accepted model to describe the origin of these sp^3 bonds is the subplantation model, in which the film grows from energetic ions, which implant themselves just below

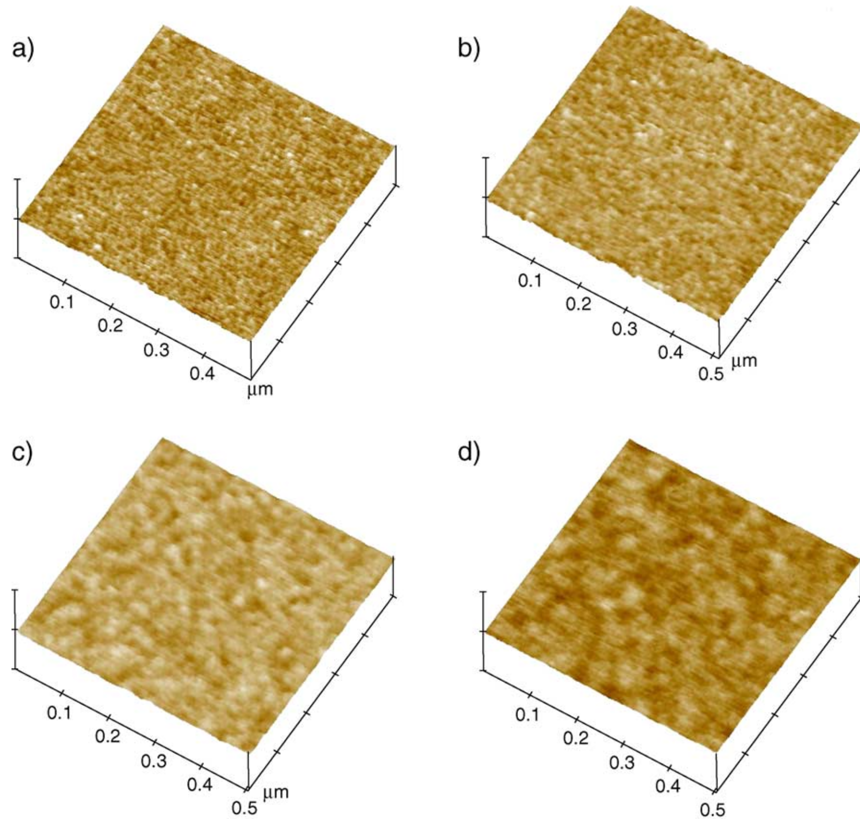

Fig. 4. AFM image of ta-C films with thickness a) 1.6 nm deposited by HCA; b) 3 nm by HCA; (c) 15nm, and (d) 60nm by FCVA. The vertical scale is 10 nm and the scan size is 0.5×0.5 μm^2.

the surface [47–49]. However, it is not subplantation itself that causes the smoothness. The mechanism of this smoothness was not previously defined, although the smoothness has been always associated experimentally with high sp^3 content [18,19].

We use a simple model to account for the smoothening process. We assume that the energy of the depositing ions dissipates locally as heat in a so-called thermal spike of ~1 ps [22] and that this heat causes a local surface melting. During this time, surface energy minimization flattens the surface locally. Fig. 7 (a,b) shows a schematic representation of the surface before and after the local melting event. We model this by a Monte Carlo simulation. The only free parameter is the number of nearest neighbours in the melted zone. We consider up to 3 nearest neighbours to be affected. We simulated films of increasing thickness up to 30 monolayers, and with a cell size of 512×512 atoms.

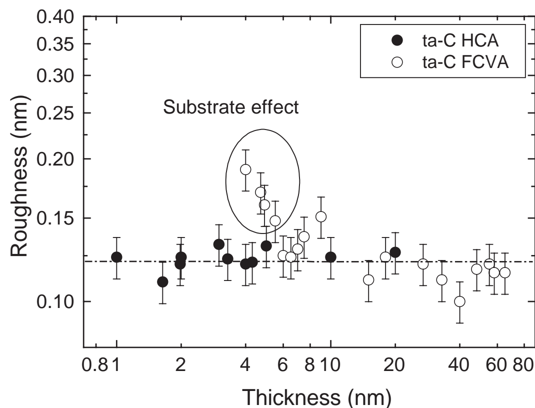

Fig. 5. Roughness evolution as a function of thickness for ta-C films deposited on Si by FCVA and HCA. Note that the roughness increase of the thinnest FCVA ta-C films is a substrate effect due to the slightly higher roughness of the Si substrate used for these films.

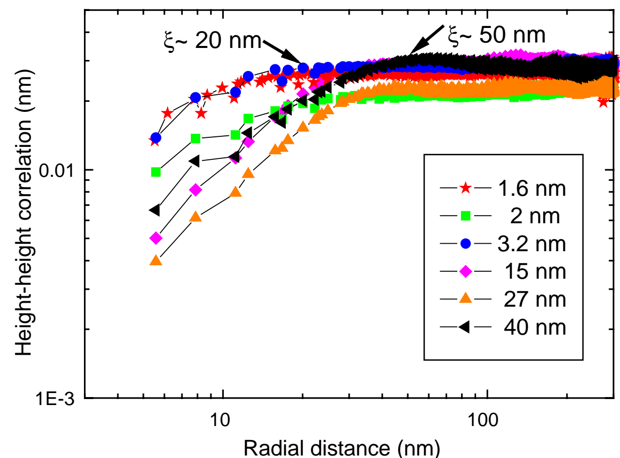

Fig. 6. Height–height correlation function for different thickness. The initial slope is related with the roughness coefficient α (Eq. (3)), while the turning point gives the correlation length, ξ (Eq. (4)). 1.6, 2 and to 3.2 nm are HCA films; 15, 27 and 40 nm are FCVA films.

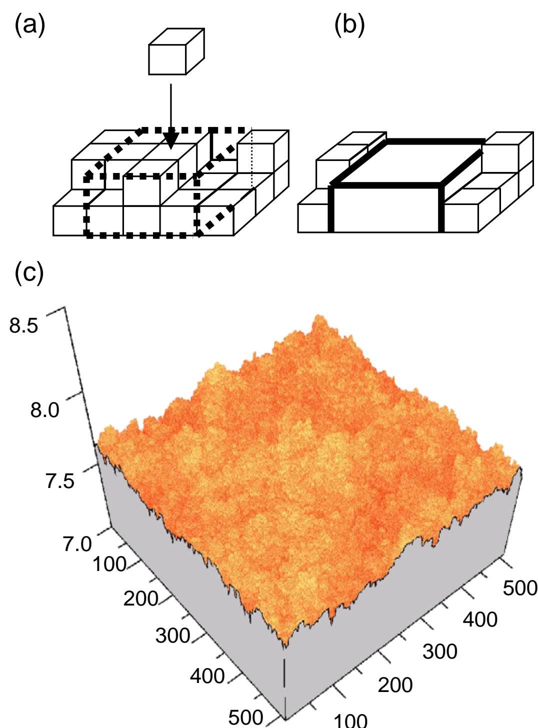

Fig. 7. Model used in the Monte-Carlo simulation (a, b) and resulting simulated surface (c), obtained by flattening of the third neighbours. (a) The energy of an incident ion is dissipated in a thermal spike volume, dot line; (b) this cause local melting and flattens the surface locally.

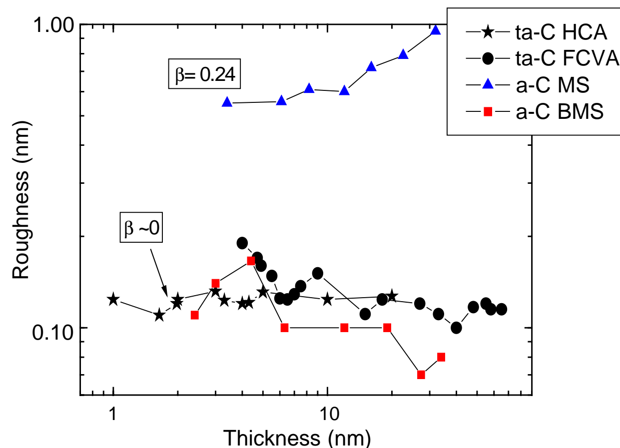

Fig. 8. Scaling law and growth exponent β for ta-C films, compared with a-C and a-C:H grown by magnetron sputtering (MS) and bias magnetron sputtering (BMS) [50]. The growth exponent for MS a-C films is ~0.24, while ~0 is for ta-C deposited by FCVA. This shows that the ion energy is a key parameter in determining the surface properties. In the case of the BMS films the roughness is constant with the thickness similar to ta-C. Actually, the heavy Ar^+ bombarding ions could in this case be effective in activating surface diffusion due to the high ion momentum, compared to C^+[51].

Fig. 7 (c) shows an example of the resulting surface. Both roughness and growth exponents slightly increase with the number of neighbours [45]. However, the scaling exponents measured on the simulated surface are in good agreement with the experimental ones.

This shows that for a fixed ion energy and room temperature, the surface properties are not related with subplantation. Actually, Raman Spectroscopy of ultra-thin ta-C films has shown that the disorder in the structure decreases below 8–10 nm [10,32,50]. This has been attributed to the cross-sectional structure evolution of ta-C films [10,32,50]. The cross-sectional structure is caused by the subplantation and is composed of: a graphitic top-layer, the bulk sp^3 rich layer and finally an interface region between the bulk and the substrate [2,47–49]. For fixed ion energy, the nature of the surface layer does not change with thickness [2]. Thus, the structural change at low thickness is related to the fact that it takes some time for the bulk layer to be formed. Thus, the thickness reduction causes a reduction in the "bulk" sp^3 phase. This simple model allows us to derive simple expressions linking the Young's modulus, density and Raman fit parameters as a function of the thickness [10,32].

The surface properties are thus not related to subplantation. This is further demonstrated in Fig. 8. We derived the growth exponent β for a-C films grown by magnetron sputtering (MS) [51]. This is ~0.24 and it matches the predictions of Kardar–Parisi–Zhang equation [39] or the molecular beam epitaxy model [37,41], Table 1. The roughness exponent would be needed in order to precisely determine the growth process. However, in both these models surface diffusion plays an important role, but the local temperature or the ion energy is not high enough to produce a viscous flux, i.e. flattening the surface. This shows that the ion energy is a key parameter in determining the surface properties, as seen in Refs. [18,19]. Samples

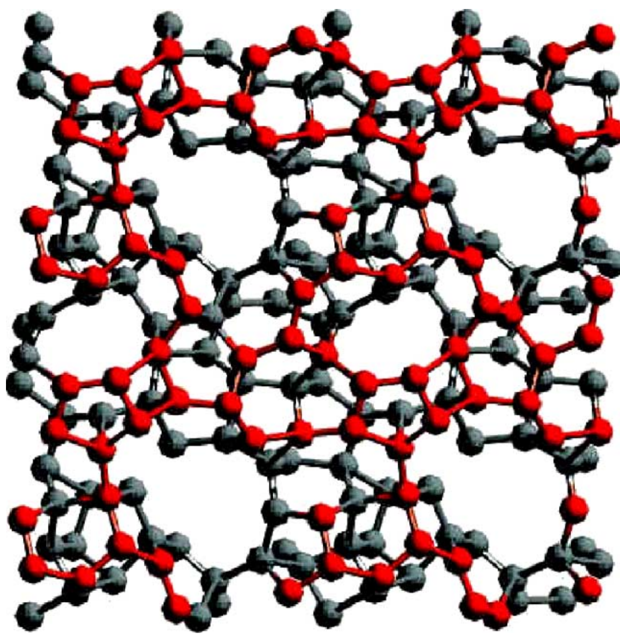

Fig. 9. Simulated surface layer of ta-C (birds-eye top down view) and its surface (red atoms), obtained by using a 200 atom supercell of ta-C of bulk density 3.2 g/cm^3 [52]. (For interpretation of the references to colour in this figure legend, the reader is referred to the web version of this article.)

deposited by magnetron sputtering assisted with Ar^+ on biased substrates (BMS) [51] show a roughness very close to ta-C (Fig. 8), apart from the initial coalescence, due to the ion damage of the substrate. Although the roughness is the same of ta-C, the density is only ~2.6 g/cm^3 [51]. Thus, the ion energy is not the only parameter in determining the surface properties. The heavy Ar^+ bombarding ions could in this case be effective in activating surface melting and diffusion due to the higher ion momentum, compared to C^+ [51]. This again supports our model.

It is interesting that the smooth ta-C films occur at a very low reduced temperature (θ), which is the deposition temperature scaled to the melting point. Assuming a melting temperature for carbon of 3000 K and room temperature as deposition temperature, the reduced temperature is θ=0.06. Diffusion and smoothening are thermally activated process. It was shown [33–35] that grain morphology in thin films varies according to the reduced temperature following the so-called 'Thornton diagrams' [33]. Surface diffusion occurs above a reduced temperature of θ~0.3. Bulk diffusion occurs above θ~0.5. Messier et al. [34] and Kelly and Arnell [35] noted that these diagrams should be generalised by introducing extra axes of ion energy and ion-to-atom flux ratio, J. The zone of surface diffusion can then fall to θ=0 for sufficient ion flux. Thus, the ion flux creates an external source of diffusion. This is in effect the situation for ta-C grown by FCVA, where J~1.

The smoothness is related to the low surface energy of ta-C. Fig. 9 shows the first monolayer (red atoms) and some lower layers (grey) of a simulated surface of ta-C. A 200 atoms supercell of ta-C of density 3.2 g/cm^3 was created and relaxed using the CASTEP plane wave pseudopotential code [52]. The cell was fractured to create two free surfaces, and the new structure and surface was relaxed. We can observe that the surface has reconstructed so that most surface atoms are three-fold coordinated and form ring-like structures with the rings parallel to the surface. This shows that the surface layer of ta-C reconstructs to form π bonded rings, where possible, to avoid any dangling bond, thus maximising its stability and minimising its surface energy. The π bonding of the surface atoms helps to form the very smooth surface. A similar surface configuration was found in earlier simulations of Kelires [24] and Dong and Drabold [25]. This monolayer reconstruction of ta-C surfaces is distinct from the ~1 nm thick sp^2-rich surface layer, which forms due to subplantation [48], whose thickness is greater and varies in proportion to the ion energy.

The final question involves the temperature dependence of roughness. It was reported that the roughness of ta-C suddenly increases to 8–30 nm when it is deposited above a critical temperature of ~150–250 °C [18,53]. This appears to contradict our model. This is resolved by noting that for room temperature deposited ta-C, the outer atomic layer reconstructs with a graphitic layer lying in the plane of the surface (Fig. 9). This allows local melting to flatten the surface. However, above the critical temperature, the bulk bonding reverts to sp^2, and the graphitic planes now lie normal to the film surface [54,55]. This creates a much larger roughness and higher surface energy.

5. Conclusion

We reviewed the kinetic surface evolution of ta-C surface and its fractal analysis. The growth exponent β is ~0–0.1, the roughness exponent α~0.39. The roughness is extremely small of order 0.1 nm. This low roughness is assigned to local melting during energetic ion deposition.

Acknowledgements

The authors wish to thank all the people involved in the work reviewed in this paper, D. Chu, A. Flewitt, D. Schneider, C. W. Chen and the team of the Mainz IBM STD plant, in particular R. Ohr and H Hilgers. The authors acknowledge the EU project FAMOUS (Project IST-2000-28661) and the project "Innovative Reaktoren und In-Situ Analytik fur nano-Schutzschichten" funded by the German Bundesministerium fur Bildung und Forschung. A. C. F. acknowledges funding from The Royal Society.

References

[1] J. Robertson, Mat. Sci. Eng. Rep. R 37 (2002) 129; Adv. Phys. 35 (1986) 317.
[2] A.C. Ferrari, A. Libassi, B.K. Tanner, V. Stolojan, J. Yuan, L.M. Brown, S.E. Rodil, B. Kleinsorge, J. Robertson, Phys. Rev., B 62 (2000) 11089.
[3] J.C. Angus, C.C. Hayman, Science 241 (1988) 913.
[4] H.W. Kroto, J.R. Heath, S.C. O'Brien, R.F. Curl, R.E. Smalley, Nature 318 (1985) 167.
[5] S. Iijima, Nature 354 (1999) 56.
[6] P.R. Goglia, J. Berkowitz, J. Hoehn, A. Xidis, L. Stover, Diamond Relat. Mater. 10 (2001) 271.
[7] R.J. Wood, IEEE Trans. Magn. 38 (2002) 1711.
[8] D. Li, M.U. Guruz, C.S. Bhatia, Y. Chung, Appl. Phys. Lett. 81 (2002) 1113.
[9] R.J. Waltman, H. Zhang, A. Khurshudov, D. Pocker, A. Karplus, B. York, Trib. Lett. 12 (2002) 51.
[10] A.C. Ferrari, Surf. Coat. Technol. 180–181 (2004) 190.
[11] F. Piazza, D. Grambole, L. Zhou, F. Talke, C. Casiraghi, A.C. Ferrari, J. Robertson, Diamond Relat. Mater. 13 (2004) 1505.
[12] J. Windeln, C. Bram, H.-L. Eckes, D. Hammel, J. Huth, J. Marien, H. Rohl, C. Schug, M. Wahl, A. Wienss, Appl. Surf. Sci. 179 (2001) 167.
[13] E.C. Cutiongco, D. Li, Y.W. Chung, C.S. Bathia, IEEE Trans. Magn. 33 (1997) 938.
[14] A. Leson, H. Hilgers, Phys. Bl. 55 (1999) 63.
[15] P. Bernhard, C. Ziethen, R. Ohr, H. Hilgers, G. Schonhense, Surf. Coat. Technol. 180 (2003) 621.
[16] H. Han, F. Ryan, M. McClure, Surf. Coat. Technol. 120 (1999) 579.
[17] C.S. Bhatia, S. Anders, I.G. Brown, K. Bobb, R. Hsiao, D.B. Bogy, J. Trib. 120 (1998) 795.
[18] Y. Lifshitz, G.D. Lempert, E. Grossman, Phys. Rev. Lett. 72 (1994) 2753.

[19] X. Shi, L. Cheah, J.R. Shi, S. Zun, B.K. Tay, J. Phys.: Condens. Matter 11 (1999) 185.
[20] H.U. Jager, K. Albe, J. Appl. Phys. 88 (2000) 1129.
[21] S. Uhlmann, T. Frauenheim, Y. Lifshitz, Phys. Rev. Lett. 81 (1998) 641.
[22] N. Marks, J. Phys.: Condens. Matter 14 (2002) 2901.
[23] R. Haerle, G. Galli, A. Baldereschi, Appl. Phys. Lett. 75 (1999) 1718.
[24] P.C. Kelires, J. Non-Cryst. Solids 227 (1998) 597.
[25] J. Dong, D.A. Drabold, Phys. Rev., B 57 (1998) 15591.
[26] R. Buzio, E. Gnecco, C. Boragno, U. Valbusa, P. Piseri, E. Barborini, P. Milani, Surf. Sci. 444 (2000) L1.
[27] E. Riedo, J. Chevrier, F. Comin, H. Brune, Surf. Sci. 477 (2001) 25.
[28] K.B.K. Teo, S.E. Rodil, J.T.H. Tsai, A.C. Ferrari, J. Robertson, W.I. Milne, J. Appl. Phys. 89 (2001) 3706;
M.C. Polo, J.L. Andujar, A. Hart, J. Robertson, W.I. Milne, Diamond Relat. Mater. 9 (2000) 663.
[29] A.C. Ferrari, J. Robertson, M.G. Beghi, C.E. Bottani, R. Ferulano, R. Pastorelli, Appl. Phys. Lett. 75 (1999) 1893.
[30] M. Beghi, A.C. Ferrari, K.B.K. Teo, J. Robertson, C.E. Bottani, A. Libassi, B.K. Tanner, Appl. Phys. Lett. 81 (2002) 3804.
[31] T. Schulke, A. Anders, P. Siemroth, IEEE Trans. Plasma Sci. 25 (1997) 660.
[32] C. Casiraghi, A.C. Ferrari, J. Robertson, R. Ohr, M.v. Gradowski, D. Schneider, H. Hilgers, Diamond Relat. Mater. 13 (2004) 1480.
[33] J.A. Thornton, J. Vac. Sci. Technol. 11 (1974) 666.
[34] R. Messier, A.P. Giri, R. Roy, J. Vac. Sci. Technol., A, Vac. Surf. Films 2 (1984) 500.
[35] P.J. Kelly, R.D. Arnell, J. Vac. Sci. Technol. A 16 (1998) 2858.
[36] F. Family, J. Phys. A 18 (1985) L75.
[37] A.-L. Barabasi, H.E. Stanley, Fractal Concepts in Surface Growth, Cambridge University Press, N. York, 1995.
[38] F. Family, T. Vicsek, Dynamics of Fractal Surfaces, World Scientific, Singapore, 1991.
[39] M. Kardar, G. Parisi, Y. Zhang, Phys. Rev. Lett. 56 (1986) 889.
[40] S. Edwards, D. Wilkinson, Proc. R. Soc. Lond., A 44 (1966) 1039.
[41] S. Das Sarma, P. Tamborenea, Phys. Rev. Lett. 66 (1991) 325.
[42] O. Rattunde, M. Moseler, A. Hafele, J. Kraft, D. Rieser, H. Haberland, J. Appl. Phys. 90 (2001) 3226.
[43] P. Bernhard, C. Ziethen, R. Ohr, H. Hilgers, G. Schonhense, Surf. Coat. Technol. 180 (2003) 621.
[44] R. Ohr, B. Jacoby, M.v. Gradowski, C. Schug, H. Hilgers, Surf. Coat. Technol. 173 (2003) 111.
[45] C. Casiraghi, A.C. Ferrari, R. Ohr, A.J. Flewitt, D.P. Chu, J. Robertson, Phys. Rev. Lett. 91 (2003) 226104.
[46] P. Tamborenea, S. Das Sarma, Phys. Rev., E Stat. Phys. Plasmas Fluids Relat. Interdiscip. Topics 48 (1993) 2575.
[47] Y. Lifshitz, S.R. Kasi, J.W. Rabalais, Phys. Rev. Lett. 62 (1989) 1290.
[48] J. Robertson, Diamond Relat. Mater. 2 (1993) 984;
Diamond Relat. Mater. 3 (1994) 361.
[49] C.A. Davis, G.A.J. Amaratunga, K.M. Knowles, Phys. Rev. Lett. 80 (1998) 3280.
[50] C. Casiraghi, A.C. Ferrari, R. Ohr, D. Chu, J. Robertson, Diamond Relat. Mater. 13 (2004) 1416.
[51] P. Patsalas, S. Logothedis, P.C. Kelires, Diamond Relat. Mater. (2005) (to be published).
[52] C. W. Chen, J. Robertson, to be published.
[53] S. Sattel, J. Robertson, H. Ehrhardt, J. Appl. Phys. 82 (1997) 4566.
[54] C.A. Davis, G.A.J. Amaratunga, K.M. Knowles, Phys. Rev. Lett. 80 (1998) 3280.
[55] Y. Yin, J. Zou, D.R. McKenzie, Nucl. Instrum. Methods B. 119 (1996) 587.